ANTIOXIDANTS & REDOX SIGNALING
Volume 17, Number 4, 2012

DOI: 10.1089/ars.2011.4239

Interactions of the Antimalarial Drug Methylene Blue with Methemoglobin and Heme Targets in *Plasmodium falciparum*: A Physico-Biochemical Study

Olga Blank, Elisabeth Davioud-Charvet, and Mourad Elhabiri

Abstract

Aims: Resistance of *Plasmodium falciparum* to drugs has led to renewed interest of redox-active methylene blue (MB) for which no resistance has been reported so far. Moreover, MB displays unique interactions with glutathione reductase (GR). However, the mechanisms of action/interaction with potential targets of MB are yet to be elucidated. Our physico-biochemical study on MB and relevant hematin-containing targets was performed under quasi-physiological conditions. ***Results:*** The water deprotonation of the Fe(III)protoporphyrin dimer, the major building block of β-hematin, was studied. At pH 6, the predominant dimer possesses water coordinated to both metals. Below pH 6, spontaneous precipitation of β-hematin occurred reminiscent of hemozoin biomineralization at pH 5.0–5.5 in the food vacuole of the malarial parasite. MB also forms dimers ($K_{Dim} = 6800\ M^{-1}$) and firmly binds to hematin in a 2:1 hematin:MB sandwich complex ($K_D = 3.16\ \mu M$). MB bioactivation catalyzed by GR induces efficient methemoglobin(Fe^{III}) [metHb(Fe^{III})] reduction to hemoglobin(Fe^{II}). The reduction rate, mediated by leucomethylene blue (LMB), was determined ($k^{metHb}_{red} = 991\ M^{-1} \cdot s^{-1}$) in an assay coupled to the GR/reduced form of nicotinamide adenine dinucleotide phosphate system. ***Innovation and Conclusion:*** Our work provides new insights into the understanding of (i) how MB interacts with hematin-containing targets, (ii) other relevant MB properties in corroboration with the distribution of the three major LMB species as a function of pH, and (iii) how this redox-active cycler induces efficient catalytic reduction of metHb(Fe^{III}) to hemoglobin(Fe^{II}) mediated by oxidoreductases. These physico-biochemical parameters of MB open promising perspectives for the interpretation of the pharmacology and pathophysiology of malaria and possibly new routes for antimalarial drug development. *Antioxid. Redox Signal.* 17, 544–554.

Introduction

Signaling by natural small molecules has become a challenging research area in the field of new antibiotic treatment of infectious diseases (48). In the last decades, important questions emerged on the other functions exerted by these small molecules at subinhibitory concentrations. Numerous redox-active molecules, in particular antibiotic phenazines, were reconsidered as key players in cell signaling, having a role in electron transfer to generate energy for growth in *Pseudomonas aeruginosa* (18, 47). In general, redox-reactive signal molecules—like phenazines and quinones—might be regarded as essential "secondary" metabolites regulating community behavior and cell–cell communication (15, 46, 60). The phenazine pyocyanin, described as the terminal signaling factor in the quorum-sensing network of *P. aeruginosa*, was recently discovered as a potent antimalarial agent (30). The "bioisosteric" behavior of its synthetic thioanalogue, methylene blue (MB; Fig. 1), known as the first industry-designed antiinfective agent, has inspired the present physicochemical study on MB and its effects on pathophysiologic mechanisms of malaria.

Malaria is a parasitic disease that is caused by *Plasmodium* species. The pathogenic agent *Plasmodium* infects humans and mosquitoes. The asexual period of the life cycle proceeds in different stages including those taking place in human erythrocytes. While the maturation of the parasite occurs in erythrocytes, from ring stage to trophozoite stages, acidic vesicles ensuring the transport of hemoglobin fuse into a single central digestive vacuole (also called food vacuole) where further digestion of hemoglobin proceeds at a pH around 5.5 (33). At this pH, oxyhemoglobin [oxyHb or oxyHb(Fe^{II})] is quickly oxidized to methemoglobin [metHb or metHb(Fe^{III})]. The binding of hemoglobin to the

Laboratoire de Chimie Bioorganique et Médicinale, European School of Chemistry, Polymers and Materials (ECPM), University of Strasbourg and Centre National de la Recherche Scientifique, Strasbourg, France.

Innovation

The therapeutical properties of methylene blue (MB) by itself are insufficient for the rapid cure of *falciparum* malaria but the lack of resistance of *Plasmodium falciparum* to MB has renewed interest in this compound and led to drug combinations of MB with amodiaquine and artesunate. The mechanisms of interaction of MB with hematin-containing targets are yet to be fully elucidated. Here, we report that MB firmly binds to the hematin π-π dimer forming a $(\text{hematin})_2$:MB complex under quasi-physiological conditions. This effect is likely to contribute to the inhibition of hemozoin formation in *P. falciparum*. In addition, it increases the concentration of parasite-toxic heme. Furthermore, we demonstrate that the reduction of methemoglobin(Fe^{III}) metHb(Fe^{III}) to oxyhemoglobin(Fe^{II}) by reduced form of nicotinamide adenine dinucleotide phosphate is efficiently catalyzed by MB and glutathione reductase, the rate constant for metHb reduction being $991 \pm 44\ M^{-1} \cdot s^{-1}$. Thus, the redox properties of MB can affect the digestion of metHb by the malarial parasites and inhibit *P. falciparum* growth. The multifaceted properties of MB will help to characterize (met)hemoglobin catabolism as an Achille's heel of *P. falciparum* and guide the design and synthesis of new and efficient redox-active drugs against malaria.

hemoglobinase falcipain-2 is strictly pH dependent, and falcipain-2 preferentially binds metHb(Fe^{III}) rather than oxyHb(Fe^{II}) (28). Inhibition of this and other proteases and its paralogues prevents parasite maturation, suggesting that drug-induced conversion of metHb(Fe^{III}) to oxyHb(Fe^{II}) may become a strategy for the design of novel antimalarial drugs.

The only part of hemoglobin not digested by *Plasmodium falciparum* is iron porphyrin (heme or PPIX). This heme is toxic because it can destabilize the membranes, inhibit enzymes, cause osmotic changes, and induce the Fenton reaction leading to the production of reactive oxygen species (ROS) inside the parasite. To detoxify hematin [=hydroxylated heme or Fe^{III}PPIX(OH) or ferriprotoporphyrin (Fe^{III}PPIX)] *Plasmodium* relies on hematin crystallization, that is the formation of hemozoin (heme biomineral or malaria pigment) (56). The stacking of iron porphyrins decreases their active surface and consequently decreases their prooxidant capacity (42). Since Fe^{II}PPIX is an inhibitor of hematin polymerization (39), redox-active compounds displaying the ability of reducing Fe^{III}PPIX to Fe^{II}PPIX can lead to the decrease of hemozoin formation and increased oxidative stress in infected red blood cells. Thus, agents with redox cycling activity able to generate Fe^{II} from Fe^{III} states either at the hemoglobin or at the heme levels might act as putative antimalarial agents by inducing the arrest of trophozoite development. Our hypothesis is that this is the main mechanism of the antimalarial action (Fig. 1) of MB (22, 51) and of the recently reported 1,4-naphthoquinones (41).

Furthermore, hemozoin production provides benefits to the parasite in suppressing the host's immune response by inhibiting macrophage functions through impaired phagocytosis after ingestion of *P. falciparum*–infected erythrocytes or isolated malarial pigment (25, 53, 54). This observation suggests that any drug able to continuously redox cycle metHb(Fe^{III}) into oxyHb(Fe^{II}), and thus to deplete the formation of hemozoin in blood stages, should contribute to reverse the depression of cellular immunity in malaria.

The redox homeostasis of *P. falciparum*–infected red blood cells is challenged with high concentration of ROS produced from the immune response of the host or from hemoglobin digestion in the parasite. The parasite prevents damage by a cytosolic antioxidant thiol network that is regenerated by two reduced forms of nicotinamide adenine dinucleotide phosphate (NADPH)–dependent disulfide oxidoreductases, GR (EC 1.8.1.7), thioredoxin reductase (EC 1.8.1.9) (32, 52), and possibly by lipoamide dehydrogenase (EC 1.8.1.4) (35).

The use of MB as an antimalarial therapeutic agent has been rediscovered a few years ago (51). Since then, further studies were performed to understand the molecular interactions of MB with potential targets, including metHb (27). Historically, the appearance of more efficient antimalarial drugs and of insecticides to combat the mosquito vector of the disease halted the use of MB. The resistance of *P. falciparum* to drugs, and the resistance of *Anopheles* to insecticides have led to the revival of MB use. No clinical resistance to MB in *P. falciparum* has been reported so far, nor could it be induced in drug pressure experiments carried out with parasites in cultures and in animal studies (58). Furthermore, MB was found active, not only against the disease-causing asexual schizonts, but also against the disease-transmitting gametocytes of *P. falciparum*: this antimalarial activity was observed both *in vitro* with all blood stages of various parasite strains in culture with 50% inhibitory concentration (IC_{50}) values in the lower nanomolar range (2) and *in vivo* (13). However, the therapeutical activity of MB alone is not sufficient to rapidly cure *falciparum* malaria in humans whereas a drug combination of MB with amodiaquine and artesunate was found to be very effective (62) and included a pronounced gametocytocidal activity. These effects recommend MB-based combinations for the control of transmission of *P. falciparum* malaria in endemic regions (13, 30). Furthermore, as early as 1891, it was reported that the phenothiazine dye MB also killed *Plasmodium vivax* (26).

The fact that MB is excreted as unmodified form, as its two electron–reduced form leucomethylene blue (LMB, Fig. 1), or as one of its demethylated metabolites (51) points out that these compounds *per se* are responsible for the drug activities of MB *in vivo*. In addition, structure-activity relationships are of particular interest since the structural properties of the heterocycle are multifaceted: MB is involved in intricate redox processes; it has the ability to change its structure pronouncedly upon reduction to LMB and both structures can be protonated in different ways. Additionally, MB and its two electron–reduced form LMB (Fig. 1) possess different lipophilicities, and MB tends to dimerize in water. MB is reduced by various NADPH-dependent disulfide reductases (9, 10), including both glutathione reductases from *Plasmodium*-infected human red blood cells (22). The flow of electrons from the nicotinamide ring of NADPH proceeds *via* the flavin ring of GR-bound FAD to the phenothiazine of MB/leucoMB. Many flavin-binding disulfide reductases show this diaphorase activity catalyzing the reduction by NAD(P)H of various dyes (MB) and quinones that act as hydrogen acceptors. Based on cysteine alkylation or Cys→Ala mutations at the active site dithiol, the NADPH-reduced flavin was shown to be the redox center for this diaphorase activity (6, 10). In particular, the deficiency of metHb(Fe^{III}) reductase (NADH

diaphorase) activity in human erythrocytes responsible for hereditary or acquired methemoglobinemia (57)—characterized by an elevated level of metHb(Fe^{III}) in erythrocytes—is corrected by MB administration (51). Redox cycling and the ability of MB to modify its lipophilicity upon electron exchange are therefore likely to form the basis for its biological effects. Revisiting the physicochemical properties and the mechanisms of action/interactions of MB toward its relevant targets might contribute to a better understanding of the physiopathology of the disease and to corroborate the concept of new redox-active agents (16, 41) against malaria.

Results

Structural and redox properties of MB

MB is based on a tricyclic phenothiazine chromophore and is an intensely colored blue cationic dye ($\varepsilon^{660} = 10^5\ M^{-1}\cdot cm^{-1}$; Fig. 1) (37). MB monomer has a characteristic absorption maximum at 665 nm. Two electron–reduced form of MB, LMB (Fig. 1), a colorless compound ($\lambda_{max} \sim 256$–262 nm), can be reoxidized by oxygen to MB. This redox cycling between MB and LMB makes MB a redox indicator, which has found many applications in bioanalytical chemistry (49, 59).

Protolytic properties of MB and LMB

MB is a positively charged cation in a wide pH range ($pK_a = 0$) (29). Under basic conditions (pH > 10–11), MB is not stable and can undergo stepwise and slow demethylation (55). By contrast, LMB could be represented by $LMBH_3^{2+}$, $LMBH_2^{+}$, LMBH, and LMB^{-} protonated species (Fig. 2). Above pH 7, LMB exists in water mainly as a deprotonated anion, LMB^{-} (29).

Dimerization of MB

The dimerization of MB in aqueous solution may appear surprising, since it possesses a positive charge, but many dyes and organic molecules display this phenomenon (38). These interactions occur in aqueous solution and have both a π-π stacking and a charge-transfer (CT) complex character (40). The nature and the concentration of electrolytes, temperature, and pH have also significant influence on the dimerization processes (45). The dimerization mechanism of MB is a two-step process involving the very fast formation of a complex from the diffusion controlled interaction of two MB molecules ($k_{1f} = 1.76\times10^9\ M^{-1}\cdot s^{-1}$, $k_{1b} = 2.23\times10^{10}\ s^{-1}$; f = forward; b = backward) followed by a slower rearrangement (k_{2f} =

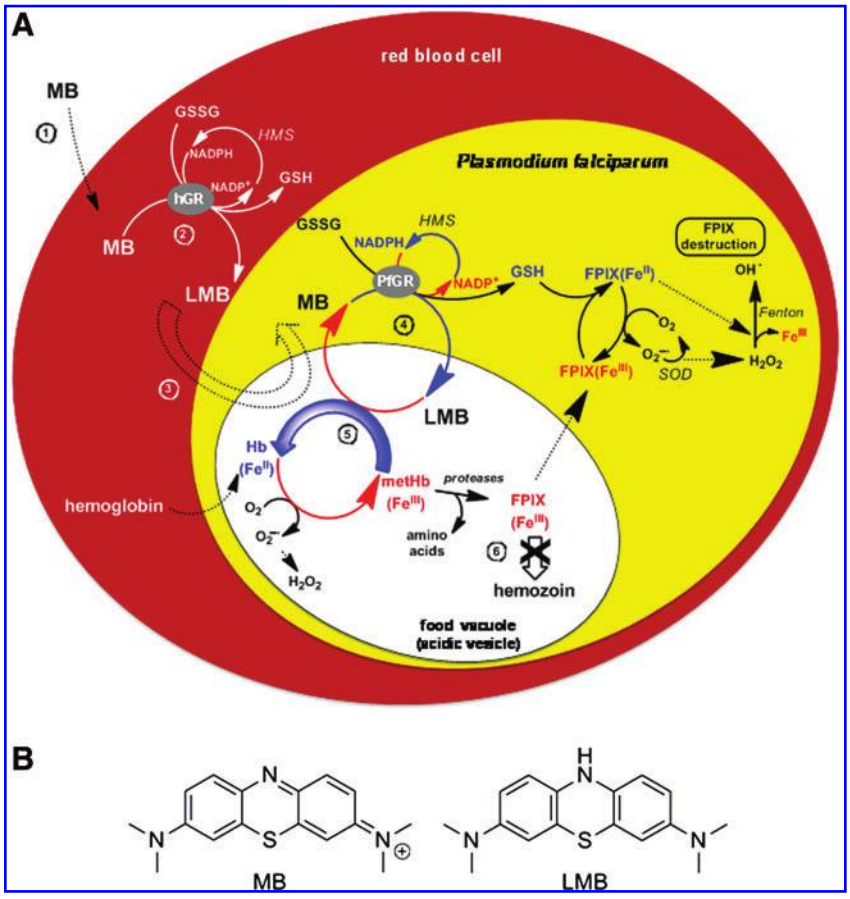

FIG. 1. Putative redox-cyling of methylene blue affecting redox homeostasis in *P. falciparum*-infected red blood cells accounting for the observed antimalarial activity. (A)** Schematic representation of the redox-cyling and trafficking processes of methylene blue. **HMS, hexose monophosphate shunt. *Blue arrows* indicate reduction; *red arrows* indicate oxidation. *Dashed arrows* represent uptake processes. MB is proposed to be taken up by the infected red blood cells (*Step 1*), to be reduced in the cytosol of the human red blood cell by *h*GR (*Step 2*), and then to be transported in the acidic vesicles or in the food vacuole (*Step 3*). Subsequently, MB is proposed to be reduced by GR of the parasite (*Step 4*) in a continuous redox cycle into the cytosols. The reduced species LMB are assumed to be transported through heme complexation into the acidic vesicles where LMB molecules transfer the electrons to oxidants [hematin or metHb(Fe^{III}), *Step 5*]. The final result is an inhibition of hemozoin formation (*Step 6*) and the arrest of trophozoite development. Thus, the antimalarial MB would act as prodrug of redox-active principles, being cycled in and out of the acidic vesicles in infected red blood cells, thereby oxidizing major intracellular reductants (NADPH) and subsequently reducing oxidants like hematin or metHb(Fe^{III}). **(B)** Chemical structures of methylene blue (MB) and its reduced form leucomethylene blue (LMB). The blue positively charged phenothiazine cation, which predominates in a wide pH range, is represented in this figure, as well as the monoprotonated and neutral LMB (in fact LMBH species). (To see this illustration in color the reader is referred to the Web version of this article at www.liebertonline.com/ars). MB, methylene blue; *h*GR, human glutathione reductase; LMB, leucomethylene blue; NADPH, reduced form of nicotinamide adenine dinucleotide phosphate; metHb(Fe^{III}), methemoglobin; LMBH, monoprotonated form of LMB.

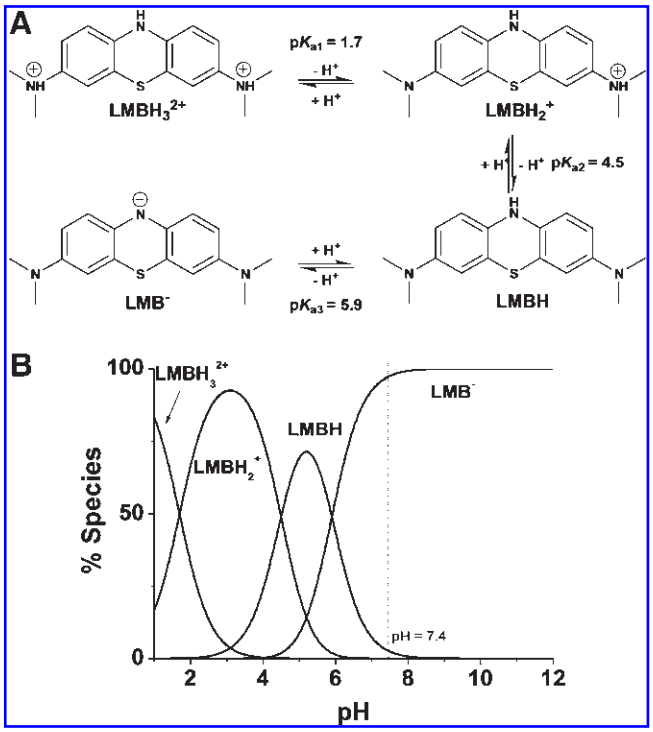

FIG. 2. Protolytic properties of leucomethylene blue (LMB) in water. (A) Acid-base equilibria of LMB in water. **(B)** Distribution diagrams of the protonated species of LMB as a function of pH calculated for $[LMB]_{tot} = 10\ \mu M$.

$6.74 \times 10^9\ s^{-1}$, $k_{2b} = 1.327 \times 10^5\ s^{-1}$) into the final stable $(MB)_2$ dimer. The two cations are arranged in a sandwich structure (45). A trimerization process was also reported and is characterized by $\beta_{Trim} = 6 \times 10^6\ M^{-2}$ (equation 1) [MB: $\lambda_{max} \sim 665$ nm; $(MB)_2$: $\lambda_{max} \sim 610$ nm, $K_{Dim} = 2000\ M^{-1}$—see equation 2; $(MB)_3$: $\lambda_{max} \sim 575$ nm, $K_{Trim} = 3000\ M^{-1}$—see equation 3] (8).

$$3\mathbf{MB} \overset{\beta_{Trim}}{\rightleftharpoons} (\mathbf{MB})_3 \qquad \text{Equation 1}$$

$$2\ \mathbf{MB} \overset{K_{Dim}}{\rightleftharpoons} (\mathbf{MB})_2 \qquad \text{Equation 2}$$

$$(\mathbf{MB})_2 + \mathbf{MB} \overset{K_{Trim}}{\rightleftharpoons} (\mathbf{MB})_3 \qquad \text{Equation 3}$$

To evaluate the K_{Dim} value under physiological conditions (pH = 7.4, $T = 37°C$), ultraviolet/visible (UV-Vis) spectra of MB were recorded at different concentrations (Fig. 3). Within the concentration range of 2.73 μM to 175 μM, a single equilibrium $2MB \rightleftarrows (MB)_2$ has been considered and higher oligomerization processes were neglected (see Supplementary Data available online at www.liebertonline.com/ars).

The absorbances at any wavelength can then be correlated to the absorptivities of both the monomer and the dimer, which are related by K_{Dim} (24).

$$A_t = \frac{1}{2}\left[\varepsilon_d C_t + \frac{(2\varepsilon_m - \varepsilon_d)\sqrt{(1 + 8K_{Dim}C_t) - 1}}{4K_{Dim}}\right] \qquad \text{Equation 4}$$

The use of equation 4 resulted in the determination of $K_{Dim} = 6.8 \times 10^3\ M^{-1}$ as well as the reconstitution of the electronic spectra of MB and $(MB)_2$ (Fig. 4). A hypsochromic shift of ~ 50 nm of the $S_0 \rightarrow S_2$ band of MB is a strong indication of a "head-to-tail" arrangement (excitonic coupling). K_{Dim} is in good agreement with the values reported in the literature measured under various experimental conditions (45).

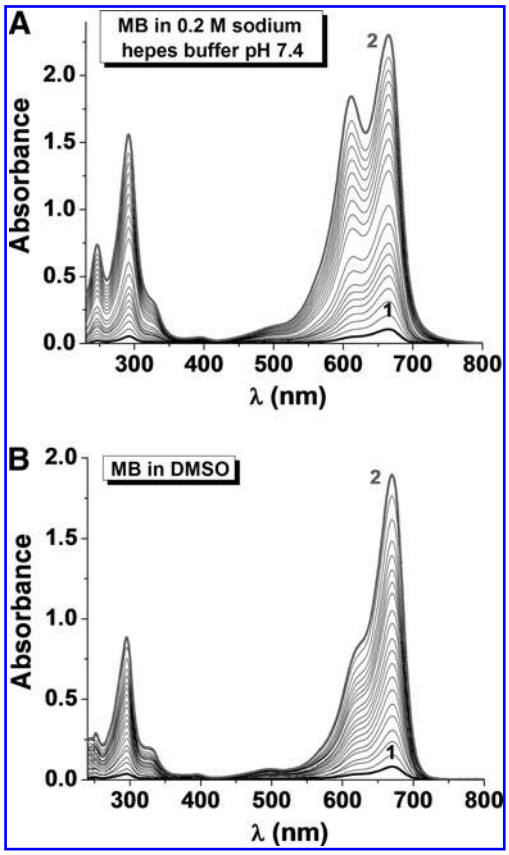

FIG. 3. Absorption spectra of MB at increasing concentration in solution. (A) 0.2 M sodium HEPES buffer of pH 7.4, $T = 37°C$; **(1)** $[MB]_{tot} = 2.73\ \mu M$; **(2)** $[MB]_{tot} = 82\ \mu M$ (data were recorded for $[MB]_{tot}$ up to 175 μM, not shown). **(B)** In DMSO, $T = 25°C$; **(1)** $[MB]_{tot} = 8\ \mu M$; **(2)** $[MB]_{tot} = 175\ \mu M$. DMSO, dimethylsulfoxide.

The distribution diagrams (Fig. 4) demonstrate the predominance of MB and $(MB)_2$. This range of concentration from 2.73 to 175 μM is relevant since MB accumulated inside the erythrocytes (36, 43). The formation of $(MB)_3$ or oligomers of higher degree is unlikely to occur *in vitro* and *in vivo* since the concentrations required in water for such processes is > 1 mM. Polymerization reactions, however, can occur in solvents of low dielectric constants such as hexane. In addition, no pH dependence on the dimerization of MB is expected because of the very low pK_a value of MB ($pK_a = 0$) (29) unless at high pH where demethylation may occur.

The dimerization was taken into account in further experiments with MB in aqueous solution, and was considered for further models for the interpretation of UV spectra. In contrast to the dimer formation in water, no dimerization was observed in dimethylsulfoxide (DMSO).

Fe^{III}PPIX in aqueous solution

In water, ferriporphyrins such as hematin can undergo various equilibria (dimerization and oligomerization) and

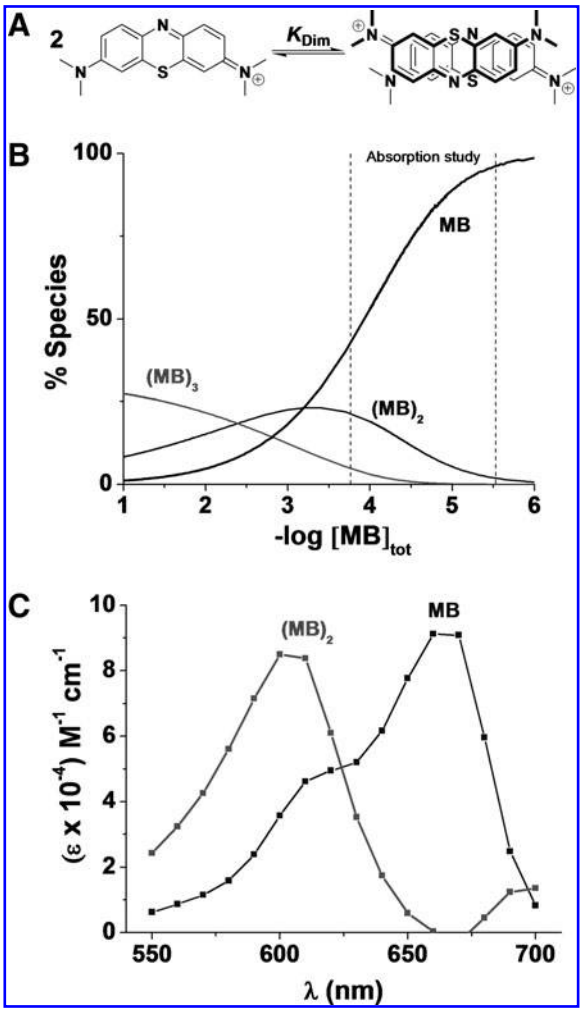

FIG. 4. Physico-chemical and absorption spectroscopic aspects of MB dimerization in pH 7.4 aqueous buffer. (A) Schematic representation of the dimer equilibrium of MB. **(B)** MB species as a function of $[MB]_{tot}$ at 37°C and pH 7.4. The trimerization constant was fixed at $K_{Trim} = 3000\ M^{-1}$. **(C)** Electronic spectra of the MB monomer and of the $(MB)_2$ dimer; Solvent: 0.2 M sodium HEPES buffer of pH 7.4, $T = 37$°C.

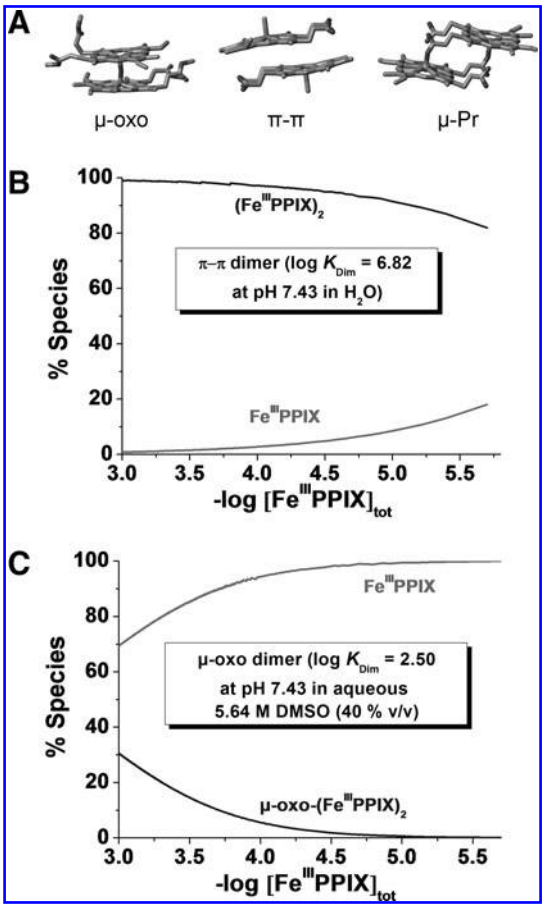

FIG. 5. Structural and physico-chemical aspects of heme self-association in aqueous solutions. (A) Molecular representations of the μ-oxo [μ-oxo-bridged iron(III) porphyrin dimer], π-π [π stacked iron(III) porphyrin dimer], and μ-Pr [dimer formed by symmetrical and mutual intermolecular iron(III)-propionate coordination bonds] arrangements of hematin in solution. Speciation diagrams of the ferriprotoporphyrin IX species as a function of $[Fe^{III}PPIX]_{tot}$ at 25°C and pH 7.4 under two solvent conditions. **(B)** In pure water; **(C)** in aqueous 5.64 M DMSO (40% v/v). $Fe^{III}PPIX$, ferriprotoporphyrin.

protolytic processes depending on the physicochemical conditions. The nature of the hematin dimer in solution has been elucidated and reviewed in the past few years (17, 31, 44). The μ-oxo dimer is the dominant species in aqueous mixtures of aprotic solvents or in detergent solutions (Fig. 5). It is characterized by an absorption band in the visible region centered at ~575 nm (4).

At pH 7.4, the π-π $(Fe^{III}PPIX)_2$ dimer represents the major species in a wide range of $[Fe^{III}PPIX]_{tot}$ (Fig. 5). The $(Fe^{III}PPIX)_2$ dimer is characterized by broad Q bands in the visible region and a CT band, (band III, $a_{2u} \rightarrow d_{yz}$) (19, 61), at ~630 nm (4). The direct overlap of the π orbitals of the porphyrins results in an excitonic coupling, which breaks the degeneracy of the excited state B, giving rise to two Soret bands lying at 385 and 360 nm. These broad and split Soret bands are spectroscopic signatures of the presence of the π-π dimer (4).

Potentiometric and absorption spectrophotometry were used to analyze the protonated species of $Fe^{III}PPIX$ present under physiological conditions (see Supplementary Data). Figure 6 displays the potentiometric titration of a 1.83 mM $(Fe^{III}PPIX)_2$ solution. Under these conditions, the $(Fe^{III}PPIX)_2$ dimer is the exclusive heme species in solution. Below pH 3, the dimer is soluble in water (dark brown color). Above pH 3 and up to pH 5–6, a brown precipitate, attributed to β-hematin (crystalline heme), is formed spontaneously. This precipitate could be resolubilized above pH 6.0. A color change from brown to green was observed when the pH was further increased to ~11.5–12, thus indicating deprotonation of the diaquo$(Fe^{III}PPIX)_2$ species. The statistical processing of the data allowed determining two pK_a values ($pK_{a1} = 7.0$ and $pK_{a2} = 8.06$). These data are in reasonable good agreement with the literature values ($pK_{a1} = 6.2$ and $pK_{a2} = 8.5$) (17).

Under basic conditions, the absorption spectrum of the $(Fe^{III}PPIX)_2$ dimer is characterized by a split B band centered at 385 and 360 nm and a CT absorption at ~611 nm. Upon protonation, marked spectral changes were observed with a red shift of ~19 nm of the CT band and a pronounced change of the relative intensities of the two Soret absorptions at

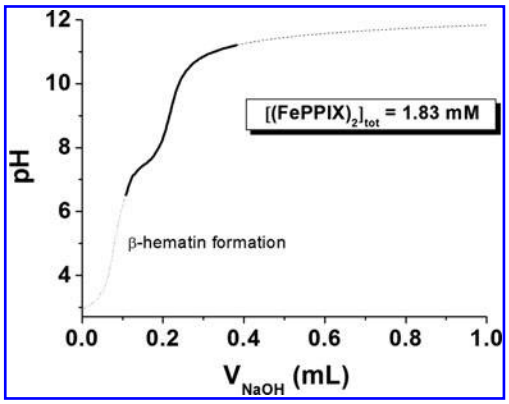

FIG. 6. Potentiometric titration curve of hematin dimer $(Fe^{III}PPIX)_2$. $T = 25°C$; $I = 0.1$ M ($NaClO_4$); $[(Fe^{III}PPIX)_2]_{tot} = 1.83$ mM. The *dotted line* (….) represents the pH region where precipitation occurs. The *solid line* (—) corresponds to the pH range for which data were processed with the Hyperquad 2000 program. The *dashed line* (——) corresponds to the pH values that were excluded from the processing.

~360–385 nm. The statistical processing of these data allowed characterizing two protonated species, $(Fe^{III}PPIX(OH))_2$ and $(Fe^{III}PPIX(OH_2))_2$, which are related by a global protonation constant $\log \beta_2 = 14.34$. This value is in agreement with the β_2 (equation 7) that can be deduced from potentiometry ($\log \beta_2 = pK_{a1} + pK_{a2} = 14.7$, equations 5 and 6).

$$(\mathbf{Fe^{III}PPIX})_2(OH_2)_2 \overset{K_{a1}}{\rightleftharpoons} (\mathbf{Fe^{III}PPIX})(OH_2) \bullet (\mathbf{Fe^{III}PPIX})(OH) + H^+ : (pK_{a1}) \quad \text{Equation 5}$$

$$(\mathbf{Fe^{III}PPIX})(OH_2) \bullet (\mathbf{Fe^{III}PPIX})(OH) \overset{K_{a2}}{\rightleftharpoons} (\mathbf{Fe^{III}PPIX})_2(OH)_2 + H^+ : (pK_{a2}) \quad \text{Equation 6}$$

$$(\mathbf{Fe^{III}PPIX})_2(OH_2)_2 \overset{\beta_2}{\rightleftharpoons} (\mathbf{Fe^{III}PPIX})_2(OH)_2 + 2H^+ : (\beta_2) \quad \text{Equation 7}$$

Electronic spectra are given in Figure 7. Deprotonation of the two water ligands induces a bathochromic shift of the CT absorption and a hyperchromic shift of the Soret bands additionally to the change in the relative absorptivities. These spectral observations can be rationalized by stronger binding of these exogenous ligands that pull outward the two ferric centers and thereby alter the π-π interactions as well as the overlap between the porphyrin, e.g., π^* excited state orbitals and the Fe^{III} d_{yz} and d_{xz} orbitals.

At pH 7.4, the mixed aquo/hydroxo complex $(Fe^{III}PPIX(OH_2))\cdot(Fe^{III}PPIX(OH))$ dominates, while the bisaquo $(Fe^{III}PPIX(OH_2))_2$ species is the major species below pH 6 (4), that is under conditions where β-hematin precipitates spontaneously. Our potentiometric study shows that the polymerization and crystallization processes may therefore be related to the formation of $(Fe^{III}PPIX(OH_2))_2$. The water molecules are more labile ligands than the hydroxyl groups. At pH < 6, the propionic side arms are deprotonated and are therefore capable to substitute the labile coordinated water ligands and to trigger the biomineralization process. The pH of the acidic digestive vacuole of *P. falciparum* is well suited for hemozoin

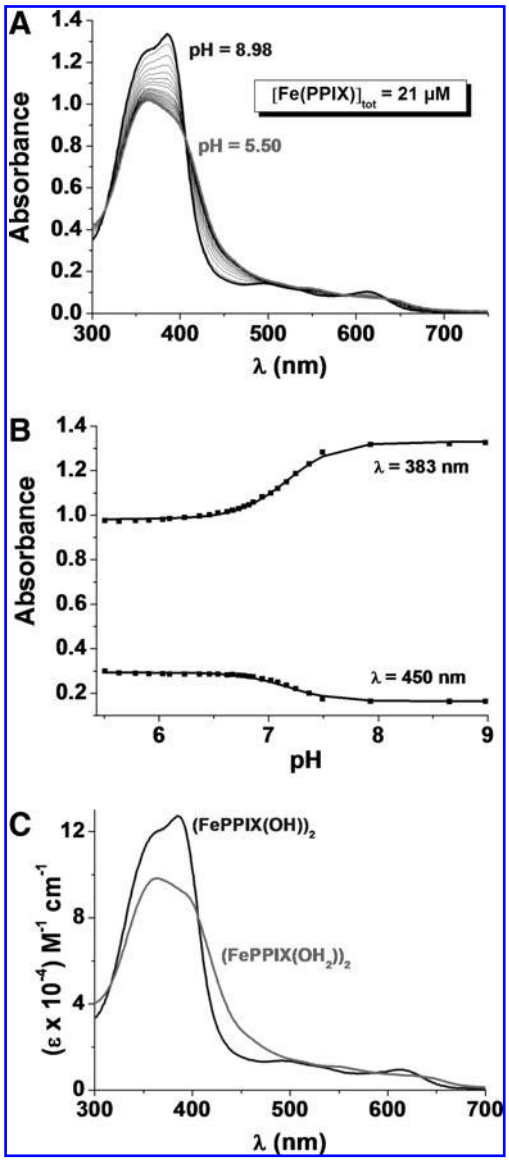

FIG. 7. UV-Vis absorption properties of the π-π hematin dimer in aqueous solution. (A) Absorption spectrophotometric titration of $Fe^{III}PPIX$ in 0.1 M $NaClO_4$ as a function of pH. **(B)** Variations of the absorbance at $\lambda = 383$ nm and at $\lambda = 450$ nm as a function of pH. **(C)** Electronic spectra of the protonated species of the hematin dimer. Solvent: water; $T = 25°C$; $l = 1$ cm; $[Fe^{III}PPIX]_{tot} = 21$ μM.

nucleation and growth, which contributes to detoxification of the large concentration of heme produced by digestion of metHb. Under more acidic conditions, dissociation can be related to the protonation of the propionates (14).

Hematin:MB speciation in aqueous solution

The inhibition of hemozoin formation is one of the targets of antimalarial therapy. The interactions between $(Fe^{III}PPIX)_2$ and MB at pH ~7.4 were first analyzed by UV-Vis absorption spectroscopy. The stoichiometry of the MB:hematin complex was determined with the method of continuous variations. Series of HEPES-buffered solutions of MB and $Fe^{III}PPIX$ subject to the condition that the sum of the total MB and $Fe^{III}PPIX$ concentrations is constant (84.1 μM) were prepared.

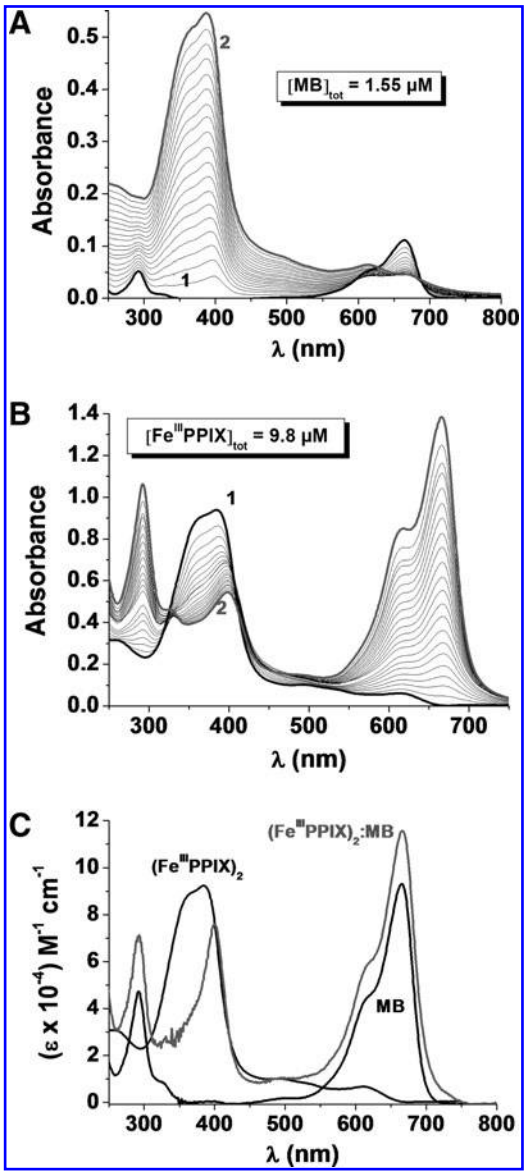

FIG. 8. UV-Vis absorption properties of the MB/π-π hematin dimer complexes in pH 7.4 aqueous buffer. (A) Spectrophotometric titration of 1.55 μM MB by $(Fe^{III}PPIX)_2$ at pH 7.4. (1) $[Fe^{III}PPIX]_{tot} = 0\ \mu M$; (2) $[Fe^{III}PPIX]_{tot} = 1.36\ \mu M$, $l = 1$ cm. **(B)** Spectrophotometric titration of 9.8 μM $Fe^{III}PPIX$ versus $[MB]_{tot}$ at pH 7.4. (1) $[MB]_{tot} = 0\ \mu M$; (2) $[MB]_{tot} = 24.8\ \mu M$, $l = 1$ cm. **(C)** Electronic spectra of MB, $(Fe^{III}PPIX)_2$ and of the MB:$(Fe^{III}PPIX)_2$ complex. Solvent: 0.2 M sodium HEPES buffer of pH 7.4, $T = 25°C$.

Absorption spectra were measured for each of the solutions and the extremum x_{max} value (~ 0.31) indicates the predominant formation of a 2:1 stoichiometry complex ($(Fe^{III}PPIX)_2$:MB).

To evaluate the affinity of MB for the hematin dimer and to get further structural and spectroscopic information, spectrophotometric titrations in the UV-Vis region were then performed at pH 7.4 (Fig. 8).

The statistical processing of the spectrophotometric data, taking into account $K_{Dim} = 6.8 \times 10^3\ M^{-1}$ for MB and $K_{Dim} = 6.6 \times 10^6\ M^{-1}$ for $Fe^{III}PPIX$ (17), led to the global (equation 8) association constant log $\beta((Fe^{III}PPIX)_2$:MB)) = 12.3 and the successive (equation 9) association constant (log $K_A = 5.5$; $K_D = 3.16\ \mu M$).

$$2\ \mathbf{Fe^{III}PPIX} + \mathbf{MB} \overset{\beta_{(Fe^{III}PPIX)_2:MB}}{\rightleftharpoons} \mathbf{(Fe^{III}PPIX)_2 : MB} \quad \text{Equation 8}$$

$$\mathbf{(Fe^{III}PPIX)_2} + \mathbf{MB} \underset{K_D}{\overset{K_A}{\rightleftharpoons}} \mathbf{(Fe^{III}PPIX)_2 : MB} \quad \text{Equation 9}$$

Binding of MB induces a significant narrowing and red shift of the Soret band of hematin. This spectroscopic finding suggests strong interactions between MB and $Fe^{III}PPIX$ and demonstrates a loss of excitonic coupling between the two ferriporphyrins, which indicates that MB is intercalated between two $Fe^{III}PPIX$ in a sandwich-type arrangement.

Since MB is a fluorescent compound ($S_2 \rightarrow S_0$ radiative deactivation at $\lambda = 685$ nm), the measurement of fluorescence spectra of the MB–hematin titration was the method of choice for an additional proof of the complex formation. The formation of $(Fe^{III}PPIX)_2$:MB was characterized by an inhibition of the MB-centered emission in agreement with π-π stacking and/or a CT between the two types of chromophores in the sandwich-like complex. The global association constant was determined to be log$\beta((Fe^{III}PPIX)_2$:MB)) = 13.1 and is in good agreement with that determined from absorption.

Methemoglobin reduction coupled assay with h*GR/NADPH*

Methemoglobin reduction by MB was reported by clinicians many years ago; its reduced metabolite LMB is the mediator *in vivo* (7). A reduction assay coupled to the human GR (*h*GR)/NADPH system *in vitro* was recently established as a relevant *in vivo* model in our laboratory (16). The reduction process of metHb(Fe^{III}) can be observed due to characteristic changes in the UV-Vis region (see Supplementary Data). The absorption spectrum of metHb(Fe^{III}) is characterized by a maximum absorption at ~ 405 nm (Soret band of the pentacoordinated Fe^{III} heme in a high spin state) and a broad band centered at ~ 603 nm. Upon metHb(Fe^{III}) reduction by LMB ($T = 25°C$; pH = 6.9), which is generated from MB by *h*GR, the formation of the reduced Hb(Fe^{II}) species was associated with a bathochromic shift of the λ_{max} of the Soret band from 405 to 410 nm (Fig. 9B). This corresponds to oxyHb(Fe^{II}) with the metal cation being hexacoordinated in a low spin state. We also observed the appearance of two new absorption bands at ~ 536 and 576 nm (Fig. 9C).

$$\text{metHb}(Fe^{III}) \rightarrow \text{Hb}(Fe^{II}) : \text{one electron - reduction rate limiting step}$$

$$\text{Hb}(Fe^{II}) + O_2 \rightarrow \text{oxyHb}(Fe^{II}) : \text{fast oxygenation step}$$

Control experiments clearly showed that in the absence of the mediation by MB and its reduced form LMB, the *h*GR/NADPH couple is not able to reduce metHb(Fe^{III}) directly (Fig. 9A). The redox cycling of MB is based on NADPH oxidation by *h*GR, which in turn catalyzes the reduction of MB to LMB ($k^{NADPH/hGR}{}_{red} = 4760\ M^{-1} \cdot s^{-1}$) (8). NADPH *per se* does not efficiently reduce MB to LMB ($k^{NADPH}{}_{red} = 6.6\ M^{-1} \cdot s^{-1}$ at pH 6.9) (10) without the enzyme *h*GR and no reduction of metHb(Fe^{III}) is observed in the absence of MB (LMB). This indicates that the *h*GR/NADPH couple is not the prevailing

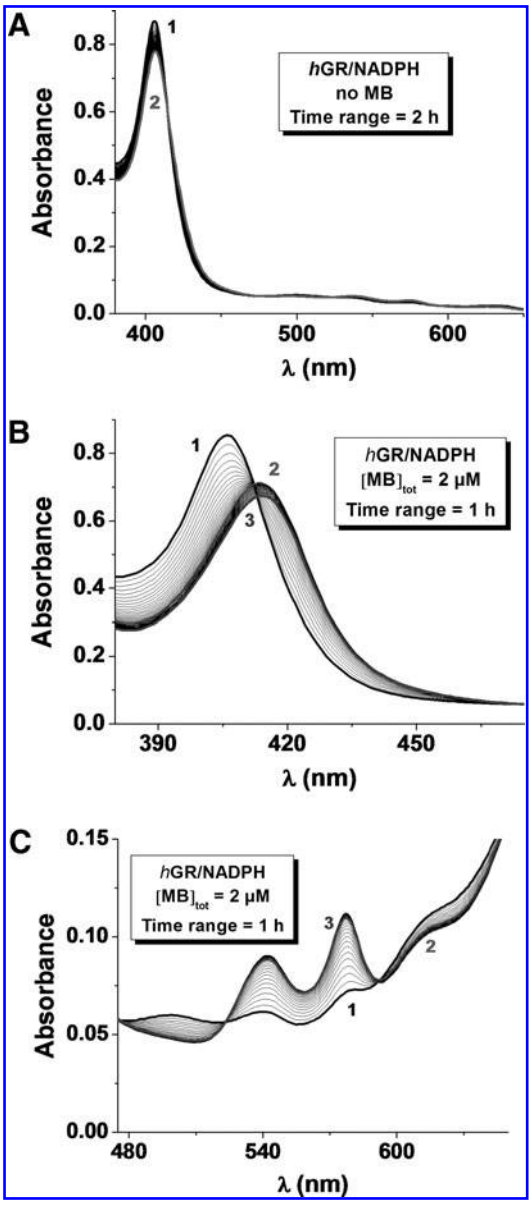

FIG. 9. Methemoglobin reduction assay using MB and *h*GR/NADPH in *h*GR buffer pH 6.9 (KH_2PO_4/K_2HPO_4, EDTA, KCl); T=25°C; $[metHb(Fe^{III})]_{tot}$=7.95 μM, $[NADPH]_{tot}$=96.5 μM, $[hGR]_{tot}$=133 nM. (A) No MB **(1)** t=0; **(2)** t=2 h. **(B)** Soret band and **(C)** absorptions bands at ~536 nm and ~576 nm for [MB]=2 μM, **(1)** t=0; **(2)** t=27 min; **(3)** t=1 h. *h*GR, human glutathione reductase; EDTA, ethylenediaminetetraacetic acid.

system but only the reductant for MB (Fig. 9). Thus, LMB is the active reducing intermediate for the reduction of metHb(Fe^{III}) to oxyHb(Fe^{II}). The splitting of the electron pair could occur at the GR-bound flavin; hence the electrons are transferred to the phenothiazine of MB and then from LMB to the heme group of metHb. Since the amount of MB used in the experiments was in some cases in the substoichiometric range $\{2.52 < [MB]_{tot}/[metHb(Fe^{III})]_{tot}{}^{mon} < 0.12\}$, and the process of metHb reduction ran to completion, the data clearly demonstrate that the redox cycling of metHb(Fe^{III}) to oxyHb(Fe^{II}) is catalytically mediated by MB through LMB generated in *h*GR-catalyzed NADPH reactions (Fig. 9). We studied metHb(Fe^{III}) reduction by varying $[MB]_{tot}$ at pH 6.9 in the presence of fixed $[hGR]_{tot}$, $[NADPH]_{tot}$, and $[metHb(Fe^{III})]_{tot}$. The apparent reduction rate (k_{obs}, s^{-1}) varied linearly with $[MB]_{tot}$ and the bimolecular reaction rate of the LMB-mediated reduction of metHb(Fe^{III}) was calculated to be $k^{metHb}{}_{red} = 991 \pm 44\ M^{-1} \cdot s^{-1}$. In the case of *P. falciparum*, the orthologous parasitic *pf*GR possesses comparable thermodynamic and kinetic properties (10).

Discussion

The determination of the physico-(bio)chemical properties of MB *in vitro* was focused on its features as an antimalarial drug. Our results led to the conclusion that MB has various profiles of action: (i) MB firmly interacts with hematin though a 2:1 sandwich complex formation and thus competes in terms of binding affinity for hematin dimers with the most potent drugs of the 4-aminoquinoline series (20, 21); (ii) MB undergoes a catalytic redox cycling that leads to efficient reduction of metHb to oxyHb through MB reduction in NADPH-dependent diaphorase-catalyzed reactions mediated by *h*GR (Figs. 1 and 9). Typical diaphorases are moonlighting flavoenzymes such as dihydrolipoamide dehydrogenase and glutathione reductase. These interactions are likely to enhance the oxidative stress for the parasite through inhibition of hemozoin formation and elevation of the hematin(Fe^{III}) concentration in the acidic digestive vesicles and vacuole.

While the MB-induced reduction of metHb(Fe^{III}) is harmful to the parasites, it is potentially beneficial for the host. The amount of metHb(Fe^{III}) is abnormally elevated in severe malaria, forming up to 16.4% of circulating hemoglobin, and also in nonparasitized human red blood cells during *P. vivax* infections (3). As reported by Anstey *et al.* (3), the degree of methemoglobinemia correlates with disease severity and severity of anemia. A decreased oxygen-carrying capacity of blood due to anemia was observed to be exacerbated by reduced oxygen-carrying capacity of metHb(Fe^{III}) (even in the presence of a low amount) contributing to tissue hypoxia in patients with severe *falciparum* malaria. *Falciparum* malaria is a major cause of morbidity and mortality in African children with severe anemia who live in malaria endemic areas. The high frequency of the sickle-cell hemoglobinopathy and of glucose-6-phosphate dehydrogenase (G6PD) enzyme deficiency in malaria endemic regions is believed to be due to a natural genetic protection against fatal malaria (1, 12, 34, 50). Evidence of G6PD deficiency in Mediterranean countries, Asia, and Sub-Sahara Africa conferring resistance against severe malaria can be explained by biochemical and clinical observations. At the biochemical level, G6PDH is the first enzyme of the pentose phosphate pathway responsible for providing the reducing power of the cells in the form of NADPH. As NADPH is the main reductant of GR in erythrocytes, G6PD deficiency in red blood cells can be regarded as *h*GR insufficiency (23). The deficiency is not lethal for humans but prevents severe attack of malaria since the oxidative stress released in erythrocytes creates a milieu hostile for *Plasmodium*. Inherited *h*GR deficiency has similar effects (23). Consequently, in these enzyme deficiency diseases and most of hemoglobinopathies, a rapid elimination of the red blood cells from the circulation occurs by enhanced phagocytosis *via*

complement activation (5, 11, 23). Increased oxidative stress in red blood cells induced by redox-active compounds like MB (23) or 1,4-naphthoquinones (41) is also expected to protect from malaria by triggering enhanced ring-stage phagocytosis rather than by impairing parasite growth directly. While MB at high dose was reported to induce hemolysis, it is important to mention that a recent clinical study in Burkina-Faso showed both efficacy and safety of the redox-active MB in G6PD-deficient patients with uncomplicated *falciparum* malaria (62).

Since the malaria treatment is faced with resistance of the parasites to various drugs, it is important to identify new targets and to reconsider old orphan drugs. MB appears to be an excellent candidate to be applied in drug combinations and to serve as the basis for the design of new redox-active substrates as novel antimalarial agents. Optimization and development of new antimalarial lead redox-active drug candidates into preclinical studies will however involve several challenges concerning the safety of patients with hemoglobinopathies and malaria.

Acknowledgments

The Centre National de la Recherche Scientifique (CNRS) and the University of Strasbourg (UMR 7509 CNRS-UdS) partly supported this work. This work was also funded by the ic-FRC (International Center for Frontier Research in Chemistry) in Strasbourg. O. B. thanks the French Embassy/Affaires Etrangères/in Berlin for granting her a postdoctoral fellowship. The authors also express their gratitude to Dr. Didier Belorgey for his careful reading of the manuscript.

Author Disclosure Statement

No competing financial interests exist for any of the authors.

References

1. Aidoo M, Terlouw DJ, Kolczak MS, McElroy PD, ter Kuile FO, Kariuki S, Nahlen BL, Lal AA, and Udhayakumar V. Protective effects of the sickle cell gene against malaria morbidity and mortality. *Lancet* 359: 1311–1312, 2002.
2. Akoachere M, Buchholz K, Fischer E, Burhenne J, Haefeli WE, Schirmer RH, and Becker K. *In vitro* assessment of methylene blue on chloroquine-sensitive and -resistant *Plasmodium falciparum* strains reveals synergistic action with artemisinins. *Antimicrob Agents Chemother* 49: 4592–4597, 2005.
3. Anstey NM, Hassanali MY, Mlalasi J, Manyenga D, and Mwaikambo ED. Elevated levels of methaemoglobin in Tanzanian children with severe and uncomplicated malaria. *Trans R Soc Trop Med Hyg* 90: 147–151, 1996.
4. Asher C, de Villiers KA, and Egan TJ. Speciation of ferriprotoporphyrin IX in aqueous and mixed aqueous solution is controlled by solvent identity, pH, and salt concentration. *Inorg Chem* 48: 7994–8003, 2009.
5. Ayi K, Turrini F, Piga A, and Arese P. Enhanced phagocytosis of ring-parasitized mutant erythrocytes: a common mechanism that may explain protection against *falciparum* malaria in sickle trait and beta-thalassemia trait. *Blood* 104: 3364–3371, 2004.
6. Bauer H, Fritz-Wolf K, Winzer A, Kühner S, Little S, Yardley V, Vezin H, Palfey B, Schirmer RH, and Davioud-Charvet E. A fluoro analogue of the menadione derivative 6-[2′-(3′-methyl)-1′,4′-naphthoquinolyl]hexanoic acid is a suicide substrate of glutathione reductase. Crystal structure of the alkylated human enzyme. *J Am Chem Soc* 128: 10784–10794, 2006.
7. Beutler E and Baluda MC. Methemoglobin reduction studies of the interaction between cell populations and of the role of methylene blue. *Blood* 22: 323–333, 1963.
8. Braswell E. Evidence for trimerization in aqueous solutions of methylene blue. *J Phys Chem* 72: 2477–2483, 1968.
9. Buchholz K, Comini MA, Wissenbach D, Schirmer RH, Krauth-Siegel RL, and Gromer S. Cytotoxic interactions of methylene blue with trypanosomatid-specific disulfide reductases and their dithiol products. *Mol Biochem Parasitol* 160: 65–69, 2008.
10. Buchholz K, Schirmer RH, Eubel JK, Akoachere MB, Dandekar T, Becker K, and Gromer S. Interactions of methylene blue with human disulfide reductases and their orthologues from *Plasmodium falciparum*. *Antimicrob Agents Chemother* 52: 183–191, 2008.
11. Cappadoro M, Giribaldi G, O'Brien E, Turrini F, Mannu F, Ulliers D, Simula G, Luzzatto L, and Arese P. Early phagocytosis of glucose-6-phosphate dehydrogenase (G6PD)-deficient erythrocytes parasitized by *Plasmodium falciparum* may explain malaria protection in G6PD deficiency. *Blood* 92: 2527–2534, 1998.
12. Cappellini MD and Fiorelli G. Glucose-6-phosphate dehydrogenase deficiency. *Lancet* 371: 64–74, 2008.
13. Coulibaly B, Zoungrana A, Mockenhaupt FP, Schirmer RH, Klose C, Mansmann U, Meissner PE, and Müller O. Strong gametocytocidal effect of methylene blue-based combination therapy against *falciparum* malaria: a randomised controlled trial. *PLoS One* 4: e5318, 2009.
14. Crespo MP, Tilley L, and Klonis N. Solution behavior of hematin under acidic conditions and implications for its interactions with chloroquine. *J Biol Inorg Chem* 15: 1009–1022, 2010.
15. Davies J. Everything depends on everything else. *Clin Microbiol Infect* 15 (Suppl. S1): 1–4, 2009.
16. Davioud-Charvet E and Lanfranchi DA. Subversive substrates of glutathione reductases from *P. falciparum*-infected red blood cells as antimalarial agents. In: *Apicomplexan Parasites—Molecular Approaches Toward Targeted Drug Development*, Volume 2, edited by Becker K; from the series *Drug Discovery in Infectious Diseases*, edited by Selzer PM. Weinheim, Germany: Wiley-VCH Verlag GmbH & Co. KGaA, 2011. ISBN 978-3-527-32731-7.
17. De Villiers KA, Kaschula CH, Egan TJ, and Marques HM. Speciation and structure of ferriprotoporphyrin IX in aqueous solution: spectroscopic and diffusion measurements demonstrate dimerization, but not μ-oxo dimer formation. *J Biol Inorg Chem* 12: 101–117, 2007.
18. Dietrich LE, Price-Whelan A, Petersen A, Whiteley M, and Newman DK. The phenazine pyocyanin is a terminal signalling factor in the quorum sensing network of *Pseudomonas aeruginosa*. *Mol Microbiol* 61: 1308–1321, 2006.
19. Eaton WA, Hanson LK, Stephens PJ, Sutherland JC, and Dunn JBR. Optical spectra of oxy- and deoxyhemoglobin. *J Am Chem Soc* 100: 4991–5003, 1978.
20. Egan TJ. Haemozoin (malaria pigment): a unique crystalline drug target. *Targets* 2: 115–124, 2003.
21. Egan TJ and Ncokasi KK. Quinoline antimalarials decrease the rate of β-hematin formation. *J Inorg Biochem* 99: 1532–1539, 2005.
22. Färber PM, Arscott LD, Williams CH Jr., Becker K, and Schirmer RH. Recombinant *Plasmodium falciparum*

glutathione reductase is inhibited by the antimalarial dye methylene blue. *FEBS Lett* 422: 311–314, 1998.
23. Gallo V, Schwarzer E, Rahlfs S, Schirmer RH, van Zwieten R, Roos D, Arese P, and Becker K. Inherited glutathione reductase deficiency and *Plasmodium falciparum* malaria—a case study. *PLoS One* 4: e7303, 2009.
24. Georges J. Deviations from Beer's law due to dimerization equilibria: theoretical comparison of absorbance, fluorescence and thermal lens measurements. *Spectrochim Acta A* 51: 985–994, 1995.
25. Green MD, Xiao L, and Lal AA. Formation of hydroxyeicosatetraenoic acids from hemozoin-catalyzed oxidation of arachidonic acid. *Mol Biochem Parasitol* 83: 183–188, 1996.
26. Guttman P and Ehrlich P. Über die wirkung des Methylenblau bei Malaria. *Berl Klin Wochenschr* 39: 953–956, 1891.
27. Haynes RK, Cheu KW, Tang MM, Chen MJ, Guo ZF, Guo ZH, Coghi P, and Monti D. Reactions of antimalarial peroxides with each of leucomethylene blue and dihydroflavins: flavin reductase and the cofactor model exemplified. *ChemMedChem* 6: 279–291, 2011.
28. Hogg T, Nagarajan K, Herzberg S, Chen L, Shen X, Jiang H, Wecke M, Blohmke C, Hilgenfeld R, and Schmidt CL. Structural and functional characterization of Falcipain-2, a hemoglobinase from the malarial parasite *Plasmodium falciparum*. *J Biol Chem* 281: 25425–25437, 2006.
29. Impert O, Katafias A, Kita P, Mills A, Pietkiewicz-Graczyk A, and Wrzeszcz G. Kinetics and mechanism of a fast leucomethylene blue oxidation by copper(II)—halide species in acidic aqueous media. *Dalton Trans* 3: 348–353, 2003.
30. Kasozi D, Gromer S, Adler H, Zocher K, Rahlfs S, Wittlin S, Fritz-Wolf K, Schirmer RH, and Becker K. The bacterial redox signaller pyocyanin as an antiplasmodial agent: comparison with its thioanalog methylene blue. *Redox Rep* 16: 154–165, 2011.
31. Klonis N, Dilanian R, Hanssen E, Darmanin C, Streltsov V, Deed S, Quiney H, and Tilley L. Hematin-hematin self-association states involved in the formation and reactivity of the malaria parasite pigment, hemozoin. *Biochemistry* 49: 6804–6811, 2010.
32. Krauth-Siegel RL, Bauer H, and Schirmer RH. Dithiol proteins as guardians of the intracellular redox milieu in parasites: old and new drug targets in trypanosomes and malaria-causing plasmodia. *Angew Chem Int Ed* 44: 690–715, 2005.
33. Lehane AM, Hayward R, Saliba KJ, and Kirk K. A verapamil-sensitive chloroquine-associated H+ leak from the digestive vacuole in chloroquine-resistant malaria parasites. *J Cell Sci* 121: 1624–1632, 2008.
34. Luzzatto L. About hemoglobins, G6PD and parasites in red cells. *Experientia* 51: 206–208, 1995.
35. McMillan PJ, Stimmler LM, Foth BJ, McFadden GI, and Müller S. The human malaria parasite *Plasmodium falciparum* possesses two distinct dihydrolipoamide dehydrogenases. *Mol Microbiol* 55: 27–38, 2005.
36. May JM, Qu Z-C, and Cobb CE. Reduction and uptake of methylene blue by human erythrocytes. *Am J Physiol Cell Physiol* 286: C1390–C1398, 2004.
37. Michaelis L and Granick S. Metachromasy of basic dyestuffs. *J Am Chem Soc* 67: 1212–1219, 1945.
38. Monk PMS, Hodgkinson NM, and Ramzan SA. Spin pairing ('dimerisation') of the viologen radical cation: kinetics and equilibria. *Dyes Pigments* 43: 207–217, 1999.
39. Monti D, Vodopivec B, Basilico N, Olliaro P, and Taramelli D. A novel endogenous antimalarial: Fe(II)-protoporphyrin IX alpha (heme) inhibits hematin polymerization to beta-hematin (malaria pigment) and kills malaria parasites. *Biochemistry* 38: 8858–8863, 1999.
40. Mukerjee P and Ghosh AK. Thermodynamic aspects of the self-association and hydrophobic bonding of methylene blue. A model system for stacking interactions. *J Am Chem Soc* 92: 6419–6424, 1970.
41. Müller T, Johann L, Jannack B, Brückner M, Lanfranchi DA, Bauer H, Sanchez C, Yardley V, Deregnaucourt C, Schrével J, Lanzer M, Schirmer RH, and Davioud-Charvet E. Glutathione reductase-catalyzed cascade of redox reactions to bioactivate potent antimalarial 1,4-naphthoquinones—a new strategy to combat malarial parasites. *J Am Chem Soc* 133: 11557–11571, 2011.
42. Oliveira MF, Timm BL, Machado EA, Miranda K, Attias M, Silva JR, Dansa-Petretski M, de Oliveira MA, de Souza W, Pinhal NM, Sousa JJ, Vugman NV, and Oliveira PL. On the pro-oxidant effects of haemozoin. *FEBS Lett* 512: 139–144, 2002.
43. Oz M, Lorke DE, Hasan M, and Petroianu GA. Cellular and molecular actions of methylene blue in the nervous system. *Med Res Rev* 31: 93–117, 2011.
44. Pagola S, Stephens PW, Bohle DS, Kosar AD, and Madsen SK. The structure of malaria pigment β-haematin. *Nature* 404: 307–310, 2000.
45. Patil K, Pawar R, and Talap P. Self-aggregation of methylene blue in aqueous medium and aqueous solutions of Bu4NBr and urea. *Phys Chem Chem Phys* 2: 4313–4317, 2000.
46. Price-Whelan A, Dietrich LE, and Newman DK. Rethinking 'secondary' metabolism: physiological roles for phenazine antibiotics. *Nat Chem Biol* 2: 71–78, 2006. Erratum in: *Nat Chem Biol* 2: 221, 2006.
47. Price-Whelan A, Dietrich LE, and Newman DK. Pyocyanin alters redox homeostasis and carbon flux through central metabolic pathways in *Pseudomonas aeruginosa* PA14. *J Bacteriol*, 189: 6372–6381, 2007.
48. Romero D, Traxler MF, López D, and Kolter R. Antibiotics as signal molecules. *Chem Rev* 111: 5492–5505, 2011.
49. Rowe A, Chuh KN, Lubin AA, Miller EA, Cook BM, Hollis DN, and Plaxco KW. Electrochemical biosensors employing an internal electrode attachment site achieve reversible, high gain detection of specific nucleic acid sequences. *Anal Chem* [Epub ahead of print];DOI: 10.1021/ac202171×, 2011.
50. Ruwende C and Hill A. Glucose-6-phosphate dehydrogenase deficiency and malaria. *J Mol Med* 76: 581–588, 1998.
51. Schirmer RH, Adler H, Pickhardt M, and Mandelkov E. "Lest we forget you—methylene blue. …" *Neurobiol Aging* 32: 2325.e7–2325.e16, 2011.
52. Schirmer RH, Müller JG, and Krauth-Siegel RL. Disulfide reductase inhibitors as chemotherapeutic agents: the design of drugs for trypanosomiasis and malaria. *Angew Chem Int Ed* 34: 141–154, 1995.
53. Schwarzer E, Turrini F, Ulliers D, Giribaldi G, Ginsburg H, and Arese P. Impairment of macrophage functions after ingestion of *Plasmodium falciparum*-infected erythrocytes or isolated malarial pigment. *J Exp Med* 176: 1033–1041, 1992.
54. Schwarzer E, Bellomo G, Giribaldi G, Ulliers D, and Arese P. Phagocytosis of malarial pigment haemozoin by human monocytes: a confocal microscopy study. *Parasitology* 123: 125–131, 2001.
55. Singhal GS and Rabinowitch E. Changes in the absoption spectrum of methylene blue with pH. *J Phys Chem* 71: 3347–3349, 1967.
56. Slater AF, Swiggard WJ, Orton BR, Flitter WD, Goldberg DE, Cerami A, and Henderson GB. An iron-carboxylate bond links the heme units of malaria pigment. *Proc Natl Acad Sci U S A* 88: 325–329, 1991.

57. Steele CW and Spink WW. Methylene blue in the treatment of poisonings associated with methemoglobinemia. *New England J Med* 208: 1152–1153, 1933.
58. Thurston JP. The chemotherapy of *Plasmodium berghei*. I. Resistance to drugs. *Parasitology* 43: 246–252, 1953.
59. Xiao Y, Lubin AA, Baker BR, Plaxco KW, and Heeger AJ. Single-step electronic detection of femtomolar DNA by target-induced strand displacement in an electrode-bound duplex. *Proc Natl Acad Sci U S A* 103: 16677–16680, 2006.
60. Yim G, Wang HH, and Davies J. Antibiotics as signalling molecules. *Philos Trans R Soc Lond B Biol Sci* 362: 1195–1200, 2007.
61. Yoshida S, Iizuka T, Nozawa T, and Hatano M. Studies on the charge transfer band in high spin state of ferric myoglobin and hemoglobin by low temperature optical and magnetic circular dichroism spectroscopy. *Biochim Biophys Acta Protein Structure* 405: 122–135, 1975.
62. Zoungrana A, Coulibaly B, Sié A, Walter-Sack I, Mockenhaupt FP, Kouyaté B, Schirmer RH, Klose C, Mansmann U, Meissner P, and Müller O. Safety and efficacy of methylene blue combined with artesunate or amodiaquine for uncomplicated *falciparum* malaria: a randomized controlled trial from Burkina Faso. *PLoS One* 3: e1630, 2008.

Address correspondence to:
Dr. Mourad Elhabiri
Laboratoire de Chimie Bioorganique et Médicinale
European School of Chemistry, Polymers and Materials (ECPM)
Université de Strasbourg and Centre
National de la Recherche Scientifique
UMR 7509 CNRS-UdS
25, rue Becquerel
Strasbourg 67087
France

E-mail: elhabiri@unistra.fr

Date of first submission to ARS Central, August 17, 2011; date of acceptance, November 6, 2011.

Abbreviations Used

ε = molar absorptivity coefficient
λ = wavelength
μ-oxo = μ-oxo-bridged iron(III) porphyrin dimer
μ-Pr = dimer formed by symmetrical and mutual intermolecular iron(III)-propionate coordination bonds
π-π = π stacked iron(III) porphyrin dimer
CT = charge transfer (complex or band)
DMSO = dimethylsulfoxide
EDTA = ethylenediaminetetraacetic acid
Fe^{III}PPIX = ferriprotoporphyrin
Fe^{III}PPIXCl = ferriprotoporphyrin chloride
G6PD = glucose-6-phosphate dehydrogenase
GR = glutathione reductase
Hb(Fe^{II}) = hemoglobin subunit
*h*GR = human glutathione reductase
*pf*GR = *Plasmodium falciparum* glutathione reductase
K_A = association constant
K_D = dissociation constant
K_{Dim} = dimerization constant
LMB = leucomethylene blue
LMBH = monoprotonated form of LMB
MB = methylene blue
metHb(Fe^{III}) = methemoglobin subunit
NADPH = reduced form of nicotinamide adenine dinucleotide phosphate
oxyHb(Fe^{II}) = hemoglobin subunit with O_2 molecule coordinated on iron(II)
ROS = reactive oxygen species
tot = total
UV-Vis = ultraviolet/visible (spectroscopy)

This article has been cited by:

1. Don Antoine Lanfranchi, Elena Cesar-Rodo, Benoît Bertrand, Hsin-Hung Huang, Latasha Day, Laure Johann, Mourad Elhabiri, Katja Becker, David L. Williams, Elisabeth Davioud-Charvet. 2012. Synthesis and biological evaluation of 1,4-naphthoquinones and quinoline-5,8-diones as antimalarial and schistosomicidal agents. *Organic & Biomolecular Chemistry* **10**:31, 6375. [CrossRef]